International Conference on Renewable Energies and Power Quality (ICREPQ'18)
Salamanca (Spain), 21th to 23th March, 2018
Renewable Energy and Power Quality Journal (RE&PQJ)
ISSN 2172-038 X, No.16 April 2018

A New LPF-Based Grid Frequency Estimation for the SOGI Filter with Improved Harmonic Rejection

J. Matas†, H. Martin†, J. Elmariachet†, A. Abusorrah* and Y. Al-Turki*,

† Department of Electric Engineering, Barcelona East School of Engineering (EEBE), Universidad Politécnica de Cataluña (UPC), Barcelona, Spain.
*Department of Electrical and Computer Engineering, King Abdulaziz University (KAU), Jeddah, Saudi Arabia.

Abstract—**This paper proposes a new method for the estimation of the grid voltage frequency using a low-pass filter (LPF) approach. The estimated frequency is used to tune a second order generalized integrator (SOGI) filter commonly used for grid monitoring purposes and applications requiring parameter estimation from the grid. A first-order LPF is used first for the estimation that behaves identically to the reported normalized SOGI-FLL. A second-order LPF is proposed instead to overcome this circumstance. The behavior of this approach is dynamically analyzed and a linearized model useful for design purposes is derived. The behavior of the proposed system is checked with simulations, showing that the model matches well with the real system and has a smoother transient response to step frequency perturbations and also a better rejection to harmonic distortion than previous approaches.**

Keywords – Grid voltage monitoring, SOGI filter, harmonic distorion, power quality.

I. INTRODUCTION

The electrical network today suffers from different kind of distortions that created a great concern about the power quality issue [1]-[3]. Power converters should estimate the parameter of the grid voltage in a context that can be polluted by harmonic distortion. Therefore, the obtained estimations can be distorted, which can be the cause of a bad inverter operation [4]-[9].

In literature the grid monitoring methods based on the SOGI filter become popular due to its easy implementation and good behavior in front of harmonic distortion [11]-[17]. These methods require of the tuning of the SOGI filter with the grid frequency in order to operate properly. This tuning had been usually performed till now using the frequency locked loop technique (FLL) proposed in [13] due to its simple structure and easy implementation. However, this tuning can be also performed now by a recent approach in [21] that uses the gradient descent method applied to the SOGI and results in three different simple gradient estimators (GE). These approaches, FLL and GE, are very simple to implement since in fact require of a single integrator and few math operations.

In [16] a linearization and gain normalization using a small signal analysis of the FLL was proposed to simplify the SOGI-FLL tuning. In [19] and [20] an additional SOGI was added as a pre-filter to the SOGI-FLL in order to provide robustness against harmonics, subharmonics, and dc-offset voltage. In these last two works a deep analysis about the SOGI trade-off between settling time response and harmonic rejection was provided for design considerations and system tuning. In [18] a complete dynamic analysis and linearization of the SOGI-FLL system was presented.

This paper presents a novel method for estimating the grid voltage frequency using a LPF and the estimated of the grid phase using the inner SOGI state variables and SOGI outputs. The LPF provides the estimated frequency to the SOGI for being adaptive with the grid frequency variations.

A first-order LPF is used first for estimating the grid frequency that results in a good system performance. However, the analysis of the system demonstrates that this approach achieves similar dynamic behavior than the normalized SOGI-FLL in [13]. So, the response to step frequency perturbations and the rejection to harmonic distortion is identical to the SOGI-FLL and both systems are equivalent.

Then, a second-order LPF is proposed for the estimation scheme. The dynamic analysis of this approach now reveals to behave with less oscillation during the transient to a step frequency perturbation than the SOGI-FLL. Moreover, the system has a better rejection to harmonics than the SOGI-FLL. Thus, it is clear that this proposal can be employed in the SOGI-related structures for improving the dynamic behavior and capability to reject harmonic distortion.

This paper is organized as follows: in section II the LPF approach and the dynamic analysis are explained. Section III shows the simulation results and section IV exposes the conclusions.

II. LPF BASED FREQUENCY ESTIMATION METHOD

The SOGI filter, Fig. 1, is a band-pass filter used in grid monitoring applications for estimating the frequency, phase and voltage amplitude of the grid. The SOGI is formed by a generalized integrator (GI) synchronized with the input voltage v_{in} by means of an outer loop between the output v_d and v_{in},

with a gain that regulates the transient response and the bandwidth of the system [12]-[21]. The SOGI provides an orthogonal output v_q, that is used with v_d for the estimation of the grid parameters.

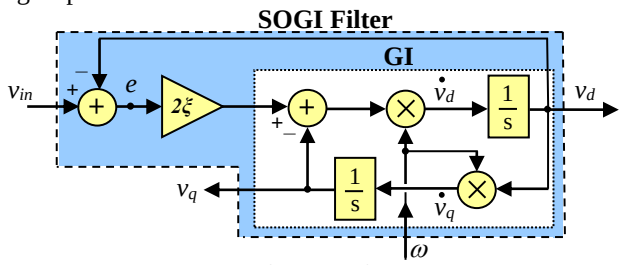

Fig. 1. Block diagram structure of the SOGI filter.

a) First-order LPF frequency estimation

The SOGI filter center frequency ω needs to be tuned with the grid frequency in order to operate well, which had been usually performed by the FLL algorithm reported in [13] and which can also be with any of the three gradient descent estimators proposed in [21]. In this paper, the frequency is obtained from direct calculations using the SOGI orthogonal outputs and some inner SOGI state variables.

Let us consider a SOGI input voltage

$$v_{in} = A_{in} sin(\omega_o t + \varphi) = A_{in} sin(\theta_o), \quad (1)$$

where A_{in}, ω_o, φ and θ_o are the amplitude, frequency, initial phase angle and phase angle of v_{in}, respectively. If the SOGI is properly tuned, i.e., $\omega = \omega_o$, the following steady state expressions will hold: $v_d = A_{in} sin(\theta_o)$, $v_q = -A_{in} cos(\theta_o)$, $\dot{v}_d = \omega_o A_{in} cos(\theta_o)$and $\dot{v}_q = \omega_o A_{in} sin(\theta_o)$.

When the former expressions for v_d, v_q and their time derivatives are substituted into the signal

$$v = v_d \cdot \dot{v}_q - \dot{v}_d \cdot v_q \,, \quad (2)$$

it is obtained

$$v = \omega_o A_{in}^2 \left(sin^2(\theta_o) + cos^2(\theta_o)\right) = \omega_o A_{in}^2 \quad (3)$$

So, the grid frequency from (3) can be obtained as

$$\omega_o = \frac{v_d \cdot \dot{v}_q - \dot{v}_d \cdot v_q}{A_{in}^2}. \quad (4)$$

With the aim of using the right hand side of (4) for tuning the SOGI center frequency ω with the grid frequency ω_o, a LPF is added in order to avoid an algebraic loop and the adverse effects of the time derivative terms in (4). The LPF will provide the average of the obtained frequency, having a filtering effect on the distortion produced by harmonics and improving the response of the SOGI to this problem. So, the frequency calculation is formulated as

$$\dot{\omega} + a \cdot \omega = a \cdot \frac{v_d \cdot \dot{v}_q - \dot{v}_d \cdot v_q}{A^2}, \quad (5)$$

where A estimates A_{in} as:

$$A^2 = v_d^2 + v_q^2 \quad (6)$$

and a is the LPF cut-off frequency in rad/s.

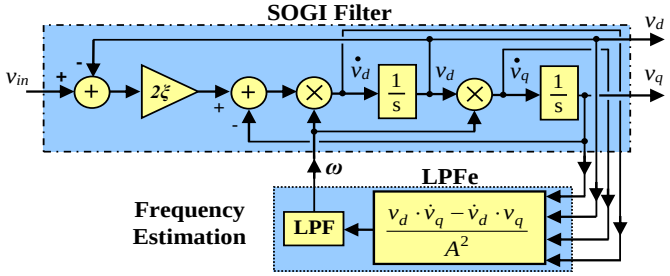

Fig. 2. Block diagram of the proposed SOGI-LPFe.

Fig. 2 depicts the block diagram of the SOGI filter with the proposed grid frequency estimator. The method will be named from now on as "LPF Frequency Estimation" (LPFe). Fig. 3 depicts the simulation results for a grid frequency step perturbation from 50Hz to 55Hz. The response of the normalized SOGI-FLL in [18] is also included in the plot for comparison purposes. The system parameters are shown in Table I.

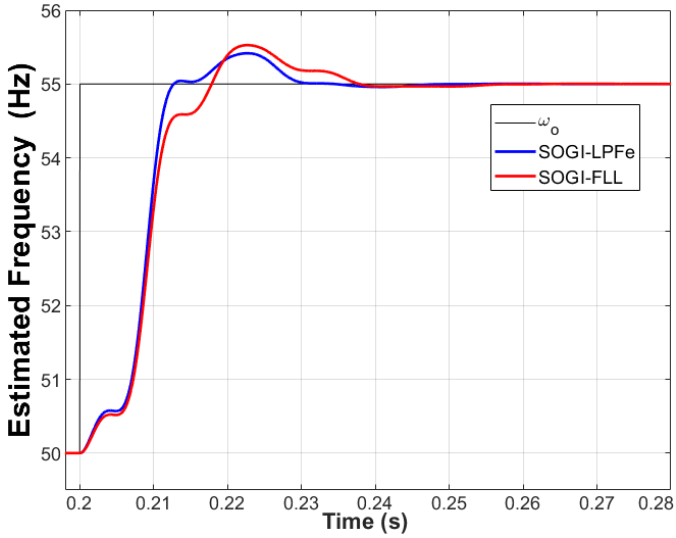

Fig. 3. Transient response of the SOGI-LPFe estimator to a grid frequency step perturbation from 50Hz to 55Hz.

TABLE. I. SOGI-LPFe AND SOGI-FLL PARAMETERS

Name	Value
SOGI-LPFe cut-off frequency, $\boldsymbol{a}$ (rad/s)	$2\pi 21$
SOGI-LPFe damping factor, $\boldsymbol{\xi}$	0.7
SOGI-FLL gain, $\boldsymbol{\lambda}$ (rad/s^2)	$157\omega_n$
SOGI-FLL, damping factor, $\boldsymbol{\xi}$	0.6
Rated grid frequency, ω_n(rad/s)	$2\pi 50$

b) LPFe System dynamics

The dynamics of the LPFe can be identified and linearized following the same procedure described in [18]. By knowing from the SOGI structure of Fig. 1 that

$$\dot{v}_d = \omega \cdot (2\xi e - v_q) \quad (7)$$

$$\dot{v}_q = \omega \cdot v_d \quad (8)$$

Equation (5) can be expressed as

$$\dot{\omega} + a\omega = a \frac{\omega \cdot [(v_d^2 + v_q^2) - 2\xi e \cdot v_q]}{A^2}. \quad (9)$$

Which, by virtue of (6) is simplified to

$$\dot{\omega} + a\omega = a \left[1 - \frac{2\xi}{A^2} e \cdot v_q\right]. \quad (10)$$

That gives the following dynamics for the frequency estimator

$$\dot{\omega} = -a \frac{2\xi}{A^2} \omega \cdot e \cdot v_q. \quad (11)$$

Complementarily, the estimated phase angle θ of v_{in} can be obtained as

$$\theta = \frac{\pi}{2} + tg^{-1} \frac{v_q}{v_d}, \quad (12)$$

whose time derivative is

$$\dot{\theta} = \frac{v_d \cdot \dot{v}_q - \dot{v}_d \cdot v_q}{A^2}. \quad (13)$$

Substituting (7)-(8) into (13) gives

$$\dot{\theta} = \omega \left[1 - \frac{2\xi}{A^2} e \cdot v_q\right]. \quad (14)$$

And taking (11) into account, it is obtained the following dynamic relationship between θ and ω

$$\dot{\theta} = \omega + \frac{1}{a}\dot{\omega} \quad (15)$$

The local asymptotic stability of the SOGI-LPFe can be assessed through its linearized small-signal model around the equilibrium point of (11). Thus, for the input in (1), assuming steady-state conditions for the fast SOGI state variables, i.e. $v_d = Asin(\theta)$ and $v_q = -Acos(\theta)$, and assuming a quasi-locked state for the LPFe, i.e., $\theta \approx \theta_o$, (11) can be developed as

$$\dot{\omega} = -a\frac{2\xi}{A^2}\omega[(A_{in}sin(\theta_o) - Asin(\theta)) \cdot (-Acos(\theta))]$$
$$= a\frac{\xi}{A}\omega \cdot [A_{in}sin(\theta_o + \theta) - Asin(2\theta) + A_{in}sin(\theta_o - \theta)] \quad (16)$$

Due to the assumed almost locked state of the system $\theta \approx \theta_o$, $A \approx A_{in}$ and applying the small-angle approximation to the trigonometric function leads to

$$\dot{\omega} = a\xi\omega\theta_e\,, \quad (17)$$

being $\theta_e \approx \theta_o - \theta$. The linearization of this small-signal frequency dynamics around the rated value of the grid frequency ω_n gives

$$\dot{\omega} = a\xi\omega_n\theta_e, \quad (18)$$

whose transfer function is

$$\omega(s) = \frac{a\xi\omega_n}{s}\theta_e(s). \quad (19)$$

Fig. 5 shows the block diagram of the SOGI-LPFe linearized model.

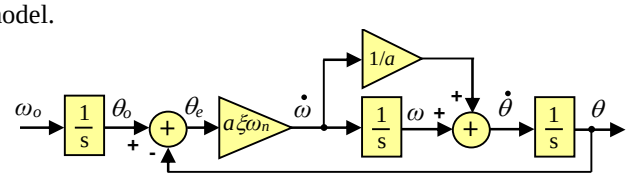

Fig. 5. Linearized model of the SOGI-LPFe using a 1st order LPF.

The system frequency and phase transfer functions are respectively

$$\frac{\omega(s)}{\omega_o(s)} = \frac{a\xi\omega_n}{s^2+\xi\omega_n s+a\xi\omega_n} \quad (20)$$

$$\frac{\theta(s)}{\theta_o(s)} = \frac{\xi\omega_n(s+a)}{s^2+\xi\omega_n s+a\xi\omega_n} \quad (21)$$

The first-order LPFe dynamics shown in (11) are identical to that of the normalized FLL in [18] if a is chosen to be $a = \lambda/(2\xi\omega_n)$, being λ the FLL gain. Therefore, it can be concluded that the LPFe proposed method is an alternative way to implement an FLL.

c) Second-order LPF approach

The behavior of the SOGI-LPFe is different if a second-order LPF with cut-off frequency a is chosen instead for filtering the frequency obtained by the right hand side of (4). Now, (10) changes to

$$\ddot{\omega} + 2a\dot{\omega} + a^2\omega = a^2\omega\left[1 - \frac{2\xi}{A^2}e \cdot v_q\right], \quad (22)$$

which simplifies to

$$\ddot{\omega} + 2a\dot{\omega} = -a^2\omega\frac{2\xi}{A^2}e \cdot v_q, \quad (23)$$

and applying the same linearization technique employed in (16)-(18) leads to the following small-signal frequency dynamics

$$\ddot{\omega} + 2a\dot{\omega} = a^2\xi\omega_n\theta_e, \quad (24)$$

whose transfer function is

$$\omega(s) = \frac{a^2\xi\omega_n}{s^2+2a\cdot s}\theta_e(s). \quad (25)$$

And the phase-to-frequency relationship results in

$$\dot{\theta} = \omega + \frac{2}{a}\dot{\omega} + \frac{1}{a^2}\ddot{\omega}. \quad (26)$$

This relationship supposes a different dynamic behavior than for the first-order LPF case. Fig. 6 depicts the block diagram of linearized model for the SOGI-LPFe using the second-order LPF.

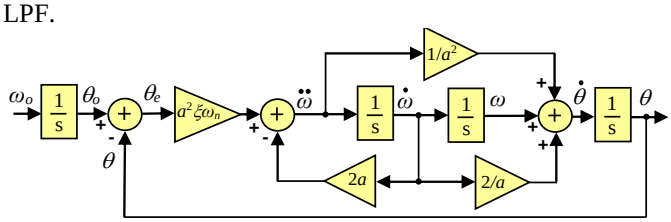

Fig. 6. Linearized model of the SOGI-LPFe using a 2nd order LPF approach.

The dynamics for the frequency and the phase can be described by the following transfer functions

$$\frac{\omega(s)}{\omega_o(s)} = \frac{a^2\xi\omega_n}{s^3+(2a+\xi\omega_n)s^2+2a\xi\omega_n s+a^2\xi\omega_n} \quad (27)$$

$$\frac{\theta(s)}{\theta_o(s)} = \frac{\xi\omega_n(s^2+2a\cdot s+a^2)}{s^3+(2a+\xi\omega_n)s^2+2a\xi\omega_n s+a^2\xi\omega_n} \quad (28)$$

The LPF is of second-order and the system dynamics are of third-order, that can be regulated by properly designing the a and ξ parameters in order to achieve a desired dynamic behavior. The design can be performed in order to achieve a specific maximum overshoot, *Mp*, and settling-time for a given frequency step transient or to limit the impact for a specific harmonic to a desired value. However, it is clear that the second-order LPF, due to its extra filtering capability, can be also designed to achieve a similar transient response than the SOGI-FLL with enhanced rejection to harmonics.

As apparent from (22), the second-order LPF employed in this section has a repeated real pole $s_{1,2} = -a$, with a as cut-off frequency and with the following transfer function

$$W(s) = \left(\frac{a}{s+a}\right)^2 = \frac{a^2}{s^2+2a\cdot s+a^2}. \quad (29)$$

However, in the design process it can be considered the use of two first-order LPFs connected in cascade instead of (29), i.e.

$$W(s) = \frac{b}{s+b}\cdot\frac{c}{s+c} = \frac{bc}{s^2+(b+c)s+bc}. \quad (30)$$

Thus, in this case, there will be two LPFs with a and b cut-off frequencies that will determine, with ξ, the transient behavior of the system. The system linearized model employing the second-order LPF in (30) corresponds to (27) and (28) but doing $a^2 = bc$ and $2a = (b + c)$.

III Simulation Results

In this section simulation results of the SOGI-LPFe with a second-order LPF and comparative results with the normalized SOGI-FLL of [18] are provided to validate the linearized model and expose the performance in face of grid harmonic distortion.

a) Linearized model validation for the 2nd-order LPFe

Fig. 7 shows the 2nd-order LPFe transient response to a grid frequency perturbation from 50Hz to 55Hz and then back to 50Hz. The parameters were ξ=0.7 and a=2π15 rad/s.

Note in this figure that the step-up and step-down responses are slightly different. For the step-up *Mp*=2.5% and peak time *tp*=0.06s and for the step-down *Mp*=3.1% and *tp*=0.059s. This phenomenon was already reported in [21] for the normalized SOGI-GE1. This phenomenon is due to the different gains that the SOGI outputs and sensed inner signals present when ω temporarily does not match ω_o. The transfer function of v_d, v_q, $\dot{v}_d$ and $\dot{v}_q$ regarding the input v_{in} are of a band-pass filter (BPF), LPF, high-pass filter (HPF) and BPF types, respectively

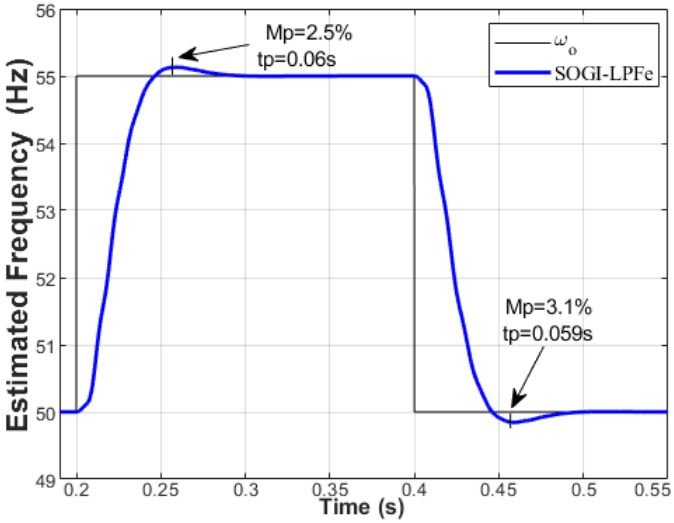

Fig. 7. Transient response of the SOGI-LPFe using a 2nd-order LPF to a frequency step perturbation from 50H to 55Hz and then back to 50Hz.

[21]. So, v_d, v_q, $\dot{v}_d$ and $\dot{v}_q$ have different gains at the two events: step-up (with $\omega_o>\omega$) and step-down (with $\omega_o<\omega$), which cause a slightly different transient behavior (see Fig. 7). In this case it should be remarked that the asymmetry found in Fig. 7 is smaller than the reported one in [21] for the normalized SOGI-GE approaches. Then, to this regard, it can be stated that the second-order LPFe has better response. Nevertheless, this asymmetry cannot be considered as a serious problem in anyone of these systems, that are mainly employed by engineers due to its structural simplicity and easy implementation.

Fig. 8 depicts the transient response of the 2nd-order SOGI-LPFe to a frequency step perturbation from 50Hz to 55Hz plotted in blue. The linearized dynamics of (27) are also plotted in red. The damping factor was fixed to ξ=0.7 and several simulations were performed for a=2π6, 2π10, 2π18 and 2π34, respectively. Note that the linearized model matches well with the real dynamics in every case.

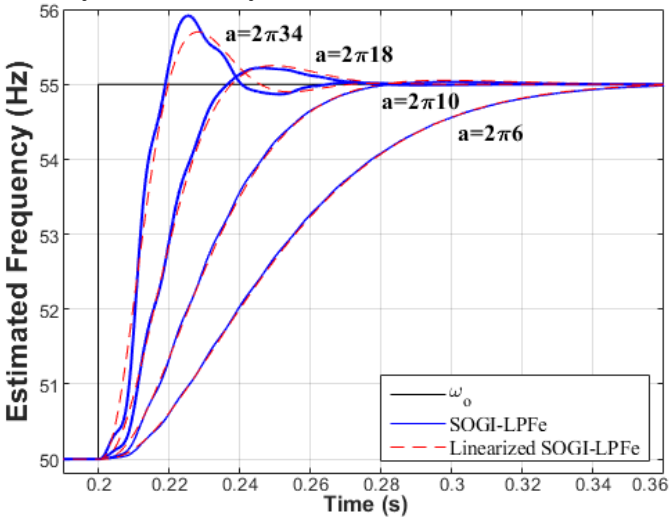

Fig. 8. Transient response to a frequency step perturbation from 50H to 55Hz, for ξ = 0.7 and a varied from 2π6 to 2π34. In blue: 2nd-order SOGI-LFPe estimated frequency. In red: Linearized 2nd-order SOGI-LFPe estimated frequency.

In contrast, Fig. 9 depicts the transient responses for the same frequency step perturbation in case of fixing a=2π6 rad/s and for varying damping factors ξ=1, 0.4 and 0.25. Moreover, Figs. 10 and 11 show detailed parts of Fig. 9. Note that as ξ decreases the maximum overshot increases. Note that the linearized model also matches well with the real dynamics, which proves that the linearized model can be used for designing the SOGI-LPFe to fulfill a desired dynamic behavior.

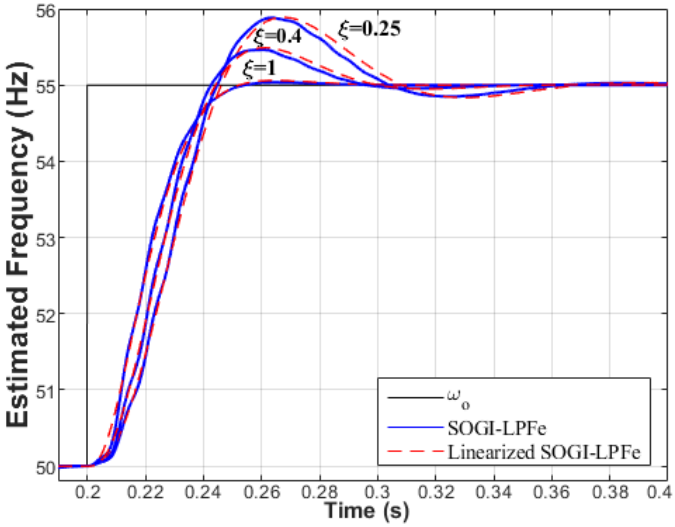

Fig. 9. Transient response to a frequency step perturbation from 50H to 55Hz, for a=2π15 and ξ varied from 0.25 to 1. In blue: 2nd-order SOGI-LFPe estimated frequency. In red: Linearized 2nd-order SOGI-LFPe estimated frequency.

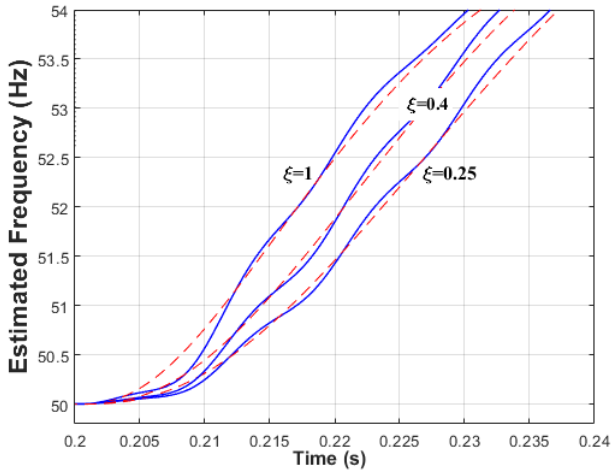

Fig. 10. Detail of Fig. 9.

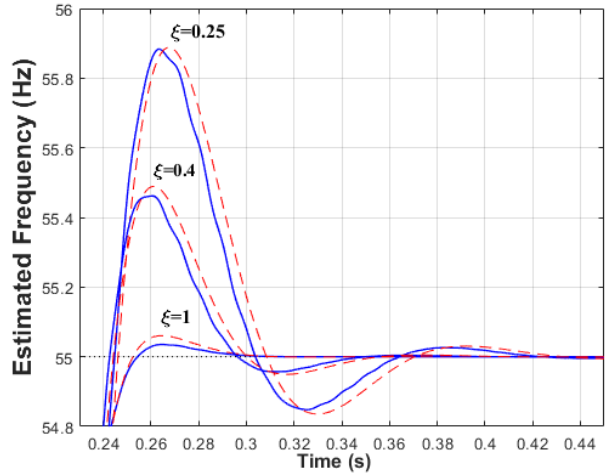

Fig. 11. Detail of Fig. 9.

b) Comparison of the 2nd-order LPFe with the FLL in terms of dynamic behavior and rejection to grid harmonics.

The 2nd-order SOGI-LPFe can be compared with the SOGI-FLL of [18] in two ways: first when they are designed using the same parameters and second for a design in which both are tuned in order to achieve the same transient response with identical maximum overshoot and peak time. The first one allows to discover the natural speed for both systems and the second one their harmonic rejection capability when having identical dynamic behavior.

The normalized SOGI-FLL estimator of [18] can be described by the following equation

$$\dot{\omega} = -\frac{\lambda}{A^2} e \cdot v_q, \tag{31}$$

where λ is the FLL gain. The linearized dynamic behavior of the SOGI-FLL to a frequency transient step perturbation is defined in (20) by considering $a = \lambda/(2\xi\omega_n)$.

Then, the 2nd-order SOGI-LPFe and the SOGI-FLL of [18] can be compared in a design that uses the same parameters, ξ and a, for both configurations. By doing that, Fig. 12 illustrates the transient behavior of both systems for the parameter pair (ξ, a)=(0.7, 2π20rad/s). The linearized dynamic versions are plotted in red.

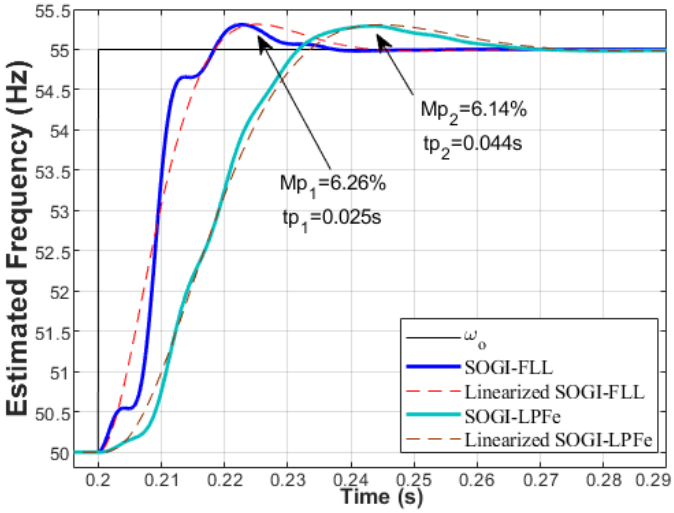

Fig. 12. Transient responses of the SOGI-FLL, the 2nd-order SOGI-LPFe and their linearized versions to a frequency step perturbation from 50H to 55Hz, with ξ=0.7 and a=2π20rad/s for all the models.

Notice in this figure that for the same ξ both systems achieve a similar *Mp* with different *tp*, being faster the SOGI-FLL. The response of the 2nd-order SOGI-LPFe is slower by 19ms. Note, in contrast, that the dynamic response of the SOGI-FLL is more oscillatory than the 2nd-order SOGI-LPFe.

Now, from the harmonic rejection point of view, Fig. 13 depicts the responses of both systems to a grid voltage affected by a 3rd harmonic distortion of 5% amplitude regarding nominal value. Notice now that the SOGI-FLL has less harmonic rejection capability than the 2nd-order SOGI-LPFe. In this case, the peak-to-peak amplitude distortion of the 2nd-order SOGI-LPFe has been reduced in -16.08 dB regarding the SOGI-FLL.

Fig. 14 depicts the transient response for both systems when they are designed in order to achieve the same transient response with *Mp*=6.14% and *tp*=0.044s, i.e., ξ=0.7 and a=2π20rad/s for the 2nd-order SOGI-LPFe and using (20), ξ=0.397 and a=2π11.26rad/s for the SOGI-FLL. Notice in this figure the oscillatory characteristics in the SOGI-FLL during the transient. Notice also how both systems match perfectly well, especially in the linearized dynamics, despite the linearized SOGI-FLL is a second-order system and the linearized SOGI-LPFe is a third-order one.

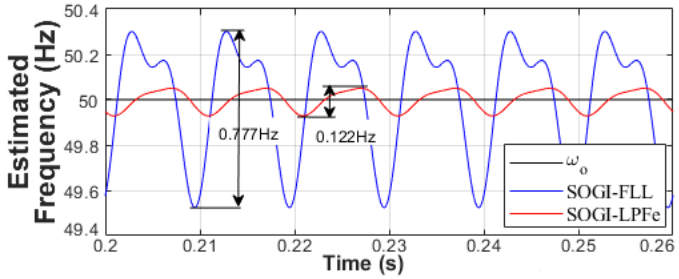

Fig. 13. Response of the SOGI-FLL and 2nd-order SOGI-LPFe to a 3rd harmonic distortion with 5% amplitude in v_{in}.

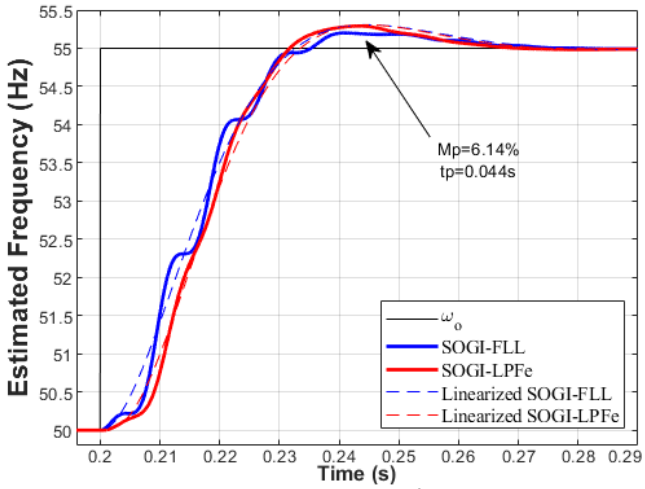

Fig. 14. Transient response SOGI-FLL, the 2nd-order SOGI-LPFe and their linearized versions to a frequency step perturbation from 50H to 55Hz, parameterized for achieving Mp=6.14% and tp=0.044s for all the models.

In order to unveil the harmonic rejection performance, Fig. 15 illustrates the response of both systems to a grid voltage with a 3rd harmonic distortion with a 5% amplitude, for the same parameterization of Fig. 14. Note in this case that the 2nd-order SOGI-LPFe still has a better rejection than the SOGI-FLL. The harmonic distortion in the 2nd-order SOGI-LPFe regarding the SOGI-FLL has been reduced in -6.45dB, which supposes a 52.3% reduction.

Finally, Fig. 16 depicts the harmonic distortion of both systems for a grid voltage with 3rd, 5th, 7th, 9th and 11th harmonics with a 5% amplitude in every simulation. The peak-to peak harmonic induced distortions in the estimated frequency have been reflected in Table II. As can be seen, the 2nd-order SOGI-LPFe has a better harmonic rejection than the SOGI-FLL, which supposes an improvement to this field.

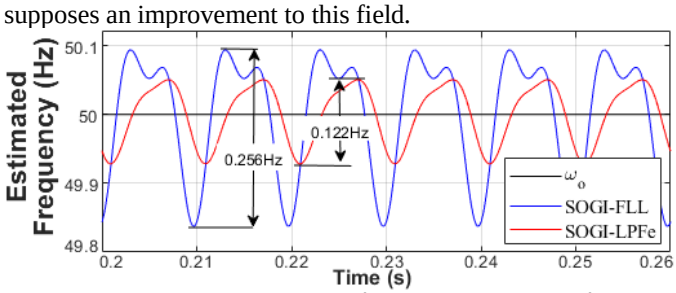

Fig. 15. Response of the SOGI-FLL and 2nd-order SOGI-LPFe to a 3rd harmonic distortion with 5% amplitude in v_{in} when they are designed in order to achieve the same transient response specifications Mp=6.14% and tp=0.044s.

As a summary, it can be stated that the 2nd-order SOGI-LPFe has the benefits of having a better rejection to harmonic distortion and a less oscillatory behavior than the SOGI-FLL during transients. The rejection to harmonics increases with the harmonic frequency order. Therefore, the 2nd-order SOGI-LPFe can be an option for enhancing the performance of the existing SOGI-based structures.

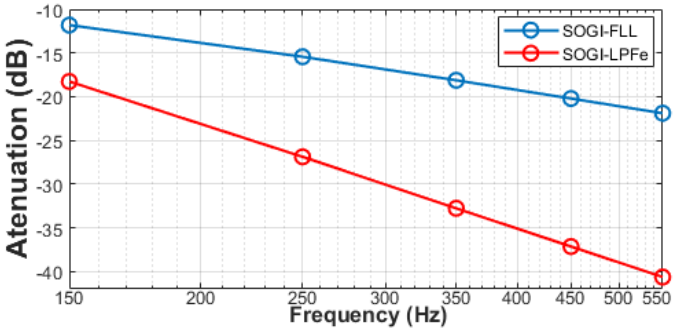

Fig. 16. Distortion amplitude in dB in the SOFI-FLL and the 2nd-order SOGI-LPFe estimated frequency for a grid voltage with harmonic distortion.

TABLE. II. PEAK-TO-PEAK AMPLITUDE DISTORTION IN THE ESTIMATED FREQUENCY FOR THE SOGI-FLL AND 2ND-ORDER SOGI-LFPe FOR DIFFERENT GRID HARMONICS ORDERS WITH 5% AMPLITUDE.

	3rd	**5th**	**7th**	**9th**	**11th**
SOGI-FLL	0.2567	0.1692	0.1241	0.0976	0.0804
SOGI-LPFe	0.1221	0.0453	0.0230	0.0139	0.0093
Reduction (dB)	-6.45	-11.45	-14.64	-16.93	-18.74
Reduction(%)	54.64	74.17	80.78	83.76	85.57

IV CONCLUSONS

In this paper a novel method for adaptively tuning the SOGI filter with the grid frequency is proposed. The method uses the estimated frequency obtained from the SOGI inner state variables and SOGI outputs plus a LPF for the proper tuning of the SOGI filter. This approach behaves identically to the normalized SOGI-FLL and presents the same small-signal linearized behavior around the rated grid frequency than the SOGI-FLL variant analyzed in [18]. Therefore, a second-order LPFe is proposed instead that behaves better than the SOGI-FLL during the grid frequency transitory perturbations and has a higher rejection to the harmonic distortion. The simulation results show that the proposed 2nd-order SOGI-LPFe has less oscillations and a smoother response than the SOGI-FLL at the event of a frequency step perturbation. Moreover, it has a higher rejection capability to harmonics than the SOGI-FLL. Therefore, it is concluded that the proposed system can be used to enhance the performance of any SOGI-based system.

REFERENCES

[1] A. Kusko, *Power quality in electrical systems*. McGraw Hill. 2007.

[2] B. Singh, A. Chandra, K. Al-Haddad, *Power quality: problems and mitigation techniques*. Wiley 2015.

[3] IEEE Standard 1547, "IEEE standard for interconnecting distributed resources with electric power systems," 2003.

[4] P. Roncero-Sanchez, X. del Toro Garcia, A. P. Torres, and V. Feliu, "Robust frequency-estimation method for distorted and imbalanced three-phase systems using discrete filters," *IEEE Trans. Power Elect.*, vol. 26, no. 4, pp. 1089-1101, Apr. 2011.

[5] J. Svensson, "Synchronization methods for grid-connected voltage source converters," *Proc. Inst. Electr. Eng. – Gener. Transm. Distrib.*, vol. 148, no. 3, pp. 229-235, May 2001.

[6] M. Karimi-Ghartemani and M.R. Iravani, "A method for synchronization of power electronic converters in polluted and variable-frequency environments," *IEEE Trans. Power Systems*, vol. 19, no. 3, pp. 1263-1270, Aug. 2004.

[7] F.D. Freijedo, J. Doval-Gandoy, O. López, and E. Acha, "Tuning of phase-locked loops for power converters under distorted utility conditions," *IEEE Trans. Ind. Appl.*, vol. 45, no. 6, pp. 2039-2047, Nov/Dec. 2009.

[8] N. Hoffmann, R. Lohde, M. Fischer, F.W. Fuchs, L. Asiminoaei, and P.B. Thogersen, "A review on fundamental grid-voltage detection methods under highly distorted conditions in distributed power-generation networks," *In proc. ECCE'11,* pp. 3045-3052, 2011.

[9] F. Gonzalez-Espin, E. Figueres, and G. Garcera, "An adaptive synchronous-reference-frame phase-locked loop for power quality improvement in a polluted utility grid," *IEEE Trans. Ind. Electron.*, vol. 59, no. 6, pp. 2718-2731, June 2012.

[10] S. Golestan, J.M. Guerrero, and J.C. Vasquez, "Single-phase PLLs: a review of recent advances," *IEEE Trans. Power Electronics*, vol. 32, no. 12, pp. 9013-9030, Dec. 2017.

[11] U. Nuβ, "Blindleistungskompensation mit selbsgeführtem stromrichter und kapazitivem energiespeicher," *Dissertation am elektrotechnischen institut der Universität Karlsruhe*, 1989.

[12] B. Burger and A. Engler, "Fast signal conditioning in single phase systems," *in Proc. EPE'01*, 2001.

[13] P. Rodriguez, A. Luna, M. Ciobotaru, R. Teodorescu, and F. Blaabjerg, "Advanced grid synchronization system for power converters under unbalanced and distorted operating conditions," *in Proc. IECON'06*, pp. 5173-5178, 2006.

[14] M. Ciobotaru, R. Teodorescu, and F. Blaabjerg, "A new single-phase PLL structure based on second order generalized integrator," *in Proc. PESC'06*, pp. 1-7, Jun. 2006.

[15] P. Rodriguez, A. Luna, I. Candela, R. Teodorescu, and F. Blaabjerg, "Grid synchronization of power converters using multiple second order generalized integrators," *in Proc. IECON'08*, pp. 755 – 760, 2008.

[16] P. Rodriguez, A. Luna, I. Candela, R. Mujal, R. Teodorescu, and F. Blaabjerg, "Multiresonant frequency-locked loop for grid synchronization of power converters under distorted grid conditions," *IEEE Trans. Ind. Electron.*, vol. 58, no. 1, pp. 127-138, Jan. 2011.

[17] P. Rodriguez, A. Luna, I. Etxebarria, R. Teodorescu, and F. Blaabjerg, "A stationary reference frame grid synchronization system for three-phase grid-connected power converters under adverse grid conditions," *IEEE Trans. Ind. Electron.*, vol. 27, no. 1, pp. 99-112, Jan. 2012.

[18] S. Golestan, E. Ebrahimzadeh, and J.M. Guerrero, and J.C. Vasquez, "An adaptive resonant regulator for single-phase grid-tied VSCs," *IEEE Trans. Power Electronics*, vol. pp, no. 99, 2017.

[19] J. Matas, M.Castilla, L.G.Vicuna, J.Miret, E.Alarcón-G., and A.Camacho, "Fast grid synchronization technique based on a multiple cascaded general integrator scheme for distributed generation inverters," *in Proc. ISIE'12*, pp.1003-1010, Jun. 2012.

[20] J. Matas, M. Castilla, J. Miret, L.G. de Vicuna, and R. Guzman, "An adaptive prefiltering method to improve the speed/accuracy tradeoff of voltage sequence detection methods under adverse grid conditions," *IEEE Trans. Ind. Electron.*, vol. 61, no. 5, pp. 2139-2151, May 2014.

[21] J. Matas, H. Martin, J. de la Hoz, A. Abusorrah, Y.A. Al-Turki, M. Al-Hindawi, "A family of gradient descent grid frequency estimators for the SOGI filter," *IEEE Trans. Power Electronics*, vol. pp, no. 99, 2017.